

better than it followed the total absorption for the incident light polarized in either direction (parallel or perpendicular to that used in the excitation spectrum). These data support the hypothesis that transitions to HES^{1,5,4} of the M center occur in the wavelength region of the F band, and that energy is not being transferred from F centers to nearby M centers (ET).⁷

The efficiency of luminescence of the M_2 transition was independent of the wavelength of the exciting light within 15% inside the quarter-maximum point on the red side, and within 11% inside the half-maximum points of the absorption curve on both sides.

The same excitation spectra showed that an M_3 transition was present and luminesced more efficiently than the M_2 transition. Excitation below 530 m μ resulted in

more efficient reorientation of the M centers than excitation above 530 m μ . It is not clear whether this is due to the M_3 and M_3' transitions affecting reorientation more than the M_2 and M_2' transitions, or to the higher energy of the exciting light.

Optical bleaching, absorption-, and excitation-spectrum experiments showed that other bands are present in NaF which have not been previously reported. There is a band on the red tail of the M band; and bands appear at 740 and 860 m μ , all of which luminesce. The 740-m μ band can be annealed out at 70°C. It is apparent that the techniques used to develop M centers in KCl cannot be carried over, unaltered, to NaF to obtain a complete conversion of F centers into M centers, with no other color centers developing.

Optical Phonons of Yttrium Aluminum Garnet

J. P. HURRELL AND S. P. S. PORTO*

Bell Telephone Laboratories, Holmdel, New Jersey

AND

I. F. CHANG AND S. S. MITRA†

Department of Electrical Engineering, ‡ University of Rhode Island, Kingston, Rhode Island

AND

R. P. BAUMAN

University of Alabama, Birmingham, Alabama

(Received 24 April 1968)

The dielectric properties and optical phonons of yttrium aluminum garnet (YAG) have been studied by measurements of the infrared (IR) reflection spectra and the Raman effect. A factor group analysis of the YAG space group shows that there are 18 T_{1u} IR-active modes, and 3 A_{1g} , 8 E_g , and 14 T_{2g} Raman-active modes. The IR data have been interpreted by a Kramers-Kronig transform to yield values of the complex dielectric constant and frequencies of the longitudinal and transverse long-wavelength T_{1u} modes. 15 of the 17 predicted T_{1u} optic modes have been observed. All the A_{1g} and E_g modes have been identified, but at least 3 of the 14 T_{2g} modes are missing from the observed Raman spectra.

I. INTRODUCTION

THE crystal structure of garnets was found by Menzer¹ to belong to the space group $Ia3d(O_h^{10})$, a body-centered cubic Bravais lattice and a member of the cubic O_h crystal class. The unit cell consists of eight molecules of $P_3Q_2(RO_4)_3$. Cations P , Q , and R have 8, 6, and 4 nearest oxygen neighbors, and are situated respectively at the 24(c), 16(a), and 24(d) sites whose positions are defined in terms of the cubic cell edge a ; the positions of the 96(h) sites of the oxygen anions

depend upon three more parameters x , y , z .² Interest in the garnets has been concentrated mainly on a few compositions for which the (a) and (d) sites have the same ions. In particular, the diamagnet yttrium aluminum garnet (YAG), $Y_3Al_2(AlO_4)_3$, and its derivatives with a rare-earth element substituting for yttrium, and the ferrimagnet yttrium iron garnet (YIG) with similar derivatives. The former system is ideal for the study of rare-earth ions in both dilute and concentrated form and is used as a host material for the neodymium 1.06- μ m laser. YIG is an important ferrite, and becomes an almost unique system for the study of indirect rare-earth-iron interactions when a rare-earth is substituted for the yttrium. Wood and

* Present address: Departments of Physics and Electrical Engineering, University of Southern California, Los Angeles, Calif.

† Work supported in part by the U. S. Air Force In-House Laboratory Independent Research Fund under Contract No. AF19-628-6042.

‡ Equipment grant from Advanced Research Projects Agency, Grant No. DA-ARO-D-31-126-G754.

¹ G. Menzer, Z. Krist. **69**, 300 (1928).

² This nomenclature and the position of the (a), (d), (c), and (h) sites can be found in the *International Tables for X-Ray Crystallography* (Kynoch Press, Birmingham, England, 1964), Vol. I.

TABLE I. Character table of reducible representations generated by arbitrary displacements of the ions. δ_{3xyz} signifies a rotation of $\frac{2}{3}\pi$ about [111]; δ_{2xy} signifies a rotation of π about [110]; δ_{2z} (δ_{4z}) signifies a rotation of π ($\frac{1}{2}\pi$) about [001]; $\tau(1) = \frac{1}{4}a$ (3,1,3); $\tau(2) = \frac{1}{2}a$ (1,0,1); $\tau(3) = \frac{1}{4}a$ (1,1,1).

O_h	Typical operation	C_1 48(<i>h</i>)	S_4 12(<i>d</i>)	D_2 12(<i>c</i>)	S_6 8(<i>a</i>)
E	$\{\epsilon 0\}$	144	36	36	24
$6C_4$	$\{\delta_{4z} \tau(1)\}$	0	0	0	0
$3C_2$	$\{\delta_{2z} \tau(2)\}$	0	-4	-4	0
$8C_3$	$\{\delta_{3xyz} 0\}$	0	0	0	0
$6C_2$	$\{\delta_{2xy} \tau(3)\}$	0	0	-4	0
I	$\{i 0\}$	0	0	0	-24
$6S_4$	$\{i\delta_{4z} \tau(1)\}$	0	-4	0	0
$3\sigma_h$	$\{i\delta_{2z} \tau(2)\}$	0	0	0	0
$8S_6$	$\{i\delta_{3xyz} 0\}$	0	0	0	0
$6\sigma_d$	$\{i\delta_{2xy} \tau(3)\}$	0	0	0	0

Remeika³ have shown that YIG is also highly transparent in the IR between about 1 and 10 μm . This window is limited at 1 μm by electronic transitions to the excited states of the trivalent iron ions and at 10 μm by the infrared-active phonons. YAG remains transparent throughout the visible region.

Previous IR studies have been made between 10 and 700 cm^{-1} of collective and single-ion excitations in rare-earth iron garnets (Wickersheim,⁴ and Sievers and Tinkham⁵) and of IR-active phonons in a variety of garnets (McDevitt⁶). In addition, Raman studies by Koningstein⁷ of electronic transitions of rare-earth ions in diamagnetic garnets have demonstrated a plethora of optical-phonon branches. We have performed an extensive investigation of the long-wavelength IR-active and Raman-active phonons in garnets. YAG was chosen as the representative garnet because of its high optical transparency and freedom from magnetic complications. In Sec. II we discuss the symmetry properties of the garnet structure appropriate to this work, and present a summary of the necessary theory to interpret the experimental results.

II. THEORY

The long-wavelength phonons can be classified according to their symmetry properties by the irreducible representations of the garnet factor group. The rows of the character table in Table I are labeled by the classes of the O_h point group followed by a typical operation of the O_h ¹⁰ factor group. The next four columns of Table I list the 80 translationally inequivalent sites in YAG according to their point symmetry and show the characters of the reducible representations generated

by their arbitrary displacements. Note that the *usual* unit cell is quoted with twice this number of occupied sites to illustrate the symmetry of the crystal rather than the full translational invariance including the equivalence of cube center and cube vertex sites.

These representations are reduced to the following:

$$48(h) \rightarrow 3(A_{1g} + A_{1u} + A_{2g} + A_{2u} + 2E_g + 2E_u + 3T_{1g} + 3T_{1u} + 3T_{2g} + 3T_{2u}),$$

$$12(d) \rightarrow A_{1u} + A_{2g} + E_g + E_u + 2T_{1g} + 3T_{1u} + 3T_{2g} + 2T_{2u},$$

$$12(c) \rightarrow A_{2g} + A_{2u} + E_g + E_u + 3T_{1g} + 3T_{1u} + 2T_{2g} + 2T_{2u},$$

$$8(a) \rightarrow A_{1u} + A_{2u} + 2E_u + 3T_{1u} + 3T_{2u}.$$

Consequently the $k \approx 0$ modes are composed of the following symmetries:

$$5A_{1u} + 3A_{1g} + 5A_{2u} + 5A_{2g} + 10E_u + 8E_g + 14T_{1g} + 18T_{1u} + 14T_{2g} + 16T_{2u}.$$

In cubic symmetry, A_{1g} , E_g , T_{2g} modes will be Raman-active and T_{1u} modes will be IR-active. The degeneracy of these T_{1u} modes is partially raised for *small* wave vectors with each mode splitting into a singly degenerate longitudinal vibration (LO) and a doubly degenerate transverse vibration (TO) under the influence of the long-range electrostatic forces. This manifests itself in the finite widths of the reststrahlen bands.

The frequencies of the TO and LO T_{1u} modes can be determined from the near normal reflection spectrum. This can be analyzed either by a multiresonance classical damped oscillator approximation to the dielectric response or a Kramers-Kronig transformation to yield the complex refractive index function directly. In the former method, the poles and zeroes of the dielectric constant are assumed to constitute TO and LO frequencies, respectively.⁸ We have adopted the latter, identifying the TO frequencies with the peaks of the optical resistivity ($nk\omega$) and the LO frequencies with the minima of the modulus of the dielectric constant ($|\epsilon|$).⁹ This method of identifying the LO modes is a suitable approximation if the modes are not heavily damped.

The Raman scattering intensity is calculated from the scattering matrices (M).¹⁰ If the incident and scattered photons have polarizations in the directions of the unit vectors \mathbf{e}_i and \mathbf{e}_s , respectively, the scattered intensity is $\alpha[\sum_{\sigma, \rho} e_i^\sigma M_{\sigma\rho} e_s^\rho]^2$. For degenerate phonons, the contributions from each scattering matrix must be added. These matrices for the Raman-active modes in

³ D. L. Wood and J. P. Remeika, J. Appl. Phys. **38**, 1038 (1967).

⁴ K. A. Wickersheim, Phys. Rev. **122**, 1376 (1961).

⁵ A. J. Sievers and M. Tinkham, Phys. Rev. **129**, 1995 (1963).

⁶ N. T. McDevitt, J. Opt. Soc. Am. **57**, 834 (1967).

⁷ J. A. Koningstein, J. Chem. Phys. **46**, 2811 (1967).

⁸ A. S. Barker, Jr., Phys. Rev. **145**, 391 (1966).

⁹ I. F. Chang and S. S. Mitra (unpublished).

¹⁰ R. Loudon, Advan. Phys. **13**, 423 (1964).

O_h symmetry are as follows:

$$A_{1g}: a_1 \begin{pmatrix} 1 & 0 & 0 \\ 0 & 1 & 0 \\ 0 & 0 & 1 \end{pmatrix}$$

$$E_g: a_{12} \begin{pmatrix} 1 & 0 & 0 \\ 0 & -1 & 0 \\ 0 & 0 & 0 \end{pmatrix}, \frac{a_{12}}{\sqrt{3}} \begin{pmatrix} 1 & 0 & 0 \\ 0 & 1 & 0 \\ 0 & 0 & -2 \end{pmatrix}$$

$$T_{2g}: a_{25} \begin{pmatrix} 0 & 1 & 0 \\ 1 & 0 & 0 \\ 0 & 0 & 0 \end{pmatrix}, a_{25} \begin{pmatrix} 0 & 0 & 1 \\ 0 & 0 & 0 \\ 1 & 0 & 0 \end{pmatrix}, a_{25} \begin{pmatrix} 0 & 0 & 0 \\ 0 & 0 & 1 \\ 0 & 1 & 0 \end{pmatrix}.$$

III. RESULTS

IR Measurements

The near normal reflection spectrum of YAG was measured at 300°K. The spectral range between 70 and 600 cm^{-1} was recorded with a Perkin Elmer model 301 far infrared spectrophotometer and the range between 400 and 4000 cm^{-1} was recorded with a Perkin Elmer model 521 infrared spectrophotometer. The frequency measurements are accurate to ~ 2 cm^{-1} and the reflection coefficient to better than 4%.

Figure 1 shows the measured reflection spectrum and Fig. 2 shows the results of the Kramers-Kronig (K-K) analysis, calculated on an IBM 360 computer. The spectrum shows 15 reflection maxima with a prominent minimum near 900 cm^{-1} . At higher frequencies the reflectivity increases monotonically to an approximately constant value of about 10% at 4000 cm^{-1} . The frequencies of the reflection peaks are listed in Table II together with the corresponding TO and LO mode frequencies obtained by the method described in the Sec. II. With one T_{1u} mode constituting the acoustic branch, 17 modes should be present in the spectrum. Presumably the two missing modes are very weak and possibly degenerate with other modes.

TO frequencies obtained from a K-K analysis are generally accurate to within the increment used for numerical integration, which in the present case was 2 cm^{-1} ; the LO frequencies identified with the minimum of $|\epsilon|$ may have a slightly higher error. It appears, however, that the TO and LO frequencies corresponding to the last three high-frequency peaks of YAG are systematically higher by some 10 or 15 cm^{-1} . This is evident from the fact that TO frequencies for relatively strong resonances should occur on the low-frequency side of a reflection peak where reflectivity rises steeply with frequency, whereas our K-K analysis gives TO frequencies identical with the frequencies of the reflection peaks. This slight error in predicting the TO frequencies is most probably due to inherent accumulated error in the K-K integration.

Raman Measurements

The Raman spectra of YAG were excited with an argon ion laser emitting about 80 mW at 4880 or 5145 Å. They were analyzed with a Spex 1400 tandem grating spectrometer and detected with a cooled EMI 6256 photomultiplier. The signals were amplified with a Keithley 610B electrometer amplifier using bandwidths of about 3 cps. Typical slit widths used were 150 μm giving a resolution of about 6 cm^{-1} .

The plane-polarized light was weakly focused inside the crystal and scattered radiation was collected perpendicular to the beam. This was focused onto the entrance slit of the spectrometer and analyzed with a polarizer placed directly in front of the entrance slit. The crystal, obtained from Linde, was cut as a 1-cm cube with {100} faces. Two opposite edges were cut away to generate two additional faces on {110} planes. This allowed the radiation to be incident along [100] and [110], which was sufficient to determine the symmetries of all the Raman-active phonons.

Figure 3 shows three typical inequivalent spectra from which the phonon symmetries can be unambiguously assigned. The contribution of different scattering symmetries is shown at the beginning of each spectrum. The spectra were recorded at $\sim 90^\circ K$. Room-

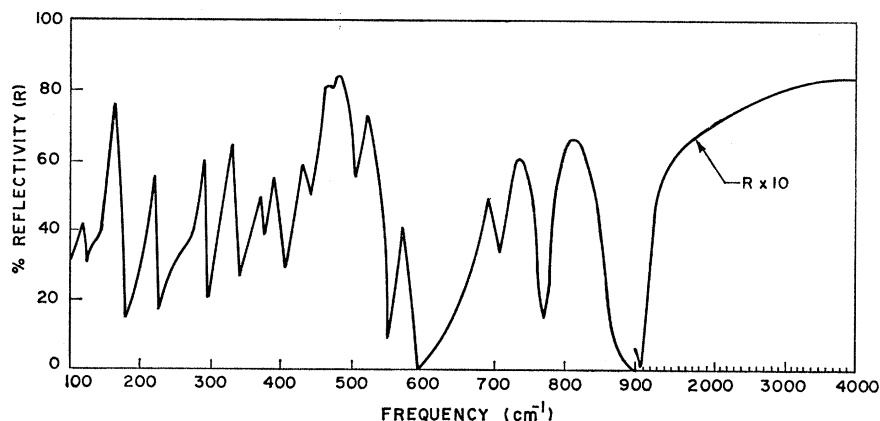


FIG. 1. Measured reflectivity of YAG. The change of scale occurs at 920 cm^{-1} .

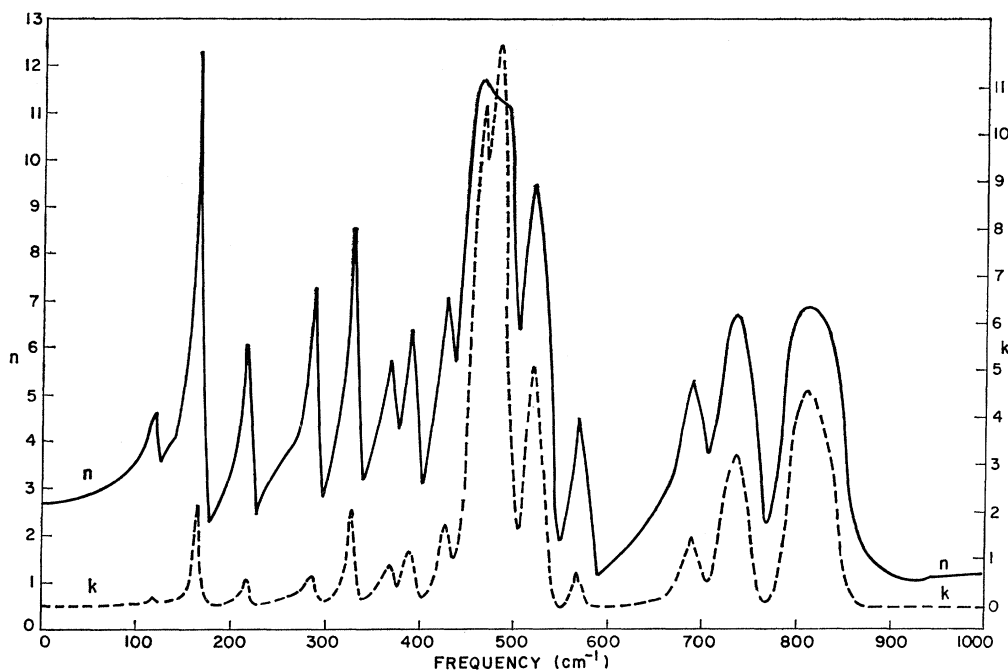


FIG. 2. Real (n) and imaginary (k) parts of the refractive index of YAG obtained from a Kramers-Kronig transform of the experimental reflectivity.

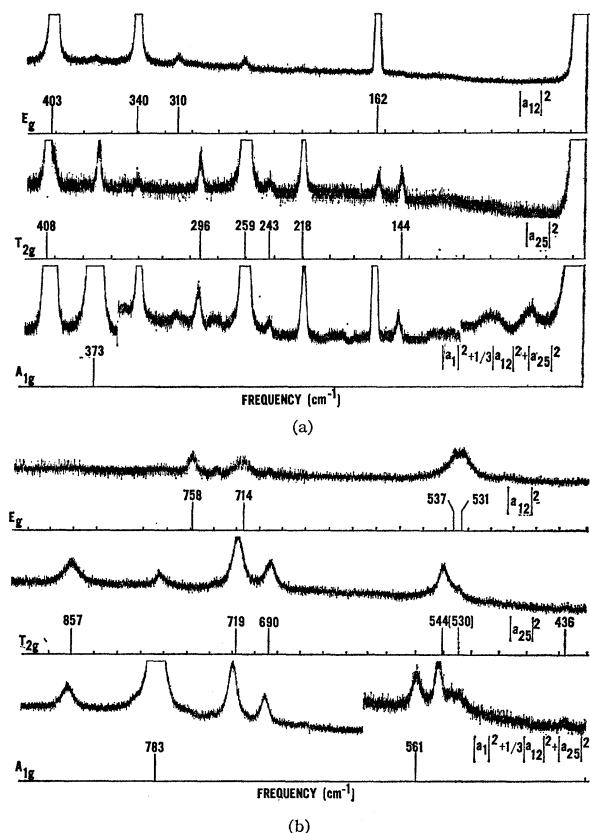


FIG. 3. (a) Measured Raman spectra of YAG between 0 and 420 cm^{-1} . The contribution from different scattering symmetries is shown at the beginning of each spectrum. The notation is defined in the text. (b) Measured Raman spectra of YAG between 420 and 900 cm^{-1} . The three traces are labeled as in Fig. 3(a).

temperature measurements showed little change in frequency though the lines were broader. Consequently, higher effective resolution was obtained at the lower temperature, enabling some overlapping lines to be more clearly resolved. Extreme weakness of many of the lines together with overlapping has made the interpretation difficult and not unambiguous. Unfortunately the strong lines show up in other polarizations, owing to incomplete collimation and misalignment, with intensities comparable with the allowed weak lines.

Two of the A_{1g} modes scatter strongly while the other is weak but definite. Three of the E_g modes scatter strongly, two weakly and three very weakly. The two weak lines are overlapping and lie close to other lines while two of the very weak lines also lie close to other strong lines. At least three of the T_{2g} modes are prob-

TABLE II. Position of reflection peaks in the IR together with derived TO and LO frequencies (in cm^{-1}).

Reflection peaks	TO modes	LO modes
120	119	125
165	165	181
219	217.8	227
290	289	298
330	329	341
370.5	370	379
392	392	403
429.5	429	437
466.5	466	471
483	482	505
520.5	521	551
570	569.5	591.8
690	690	707
737	737	769
812	811	921

Teller (LST) relation.¹⁴ This has been generalized to cubic crystals which are not diagonally cubic by Cochran¹⁵ and Cochran and Cowley¹⁶ and shown to have the form

$$\prod_j \left(\frac{\omega_{LO^j}}{\omega_{TO^j}} \right)^2 = \frac{\epsilon_0}{\epsilon_\infty}. \quad (1)$$

The values of ϵ_0 and ϵ_∞ can be calculated from the reflectivity at low and high frequencies, respectively, giving $\epsilon_0=11.7$, $\epsilon_\infty=3.65$, and hence a value 3.20 for $\epsilon_0/\epsilon_\infty$. Assuming the two missing T_{1u} modes have very weak oscillator strengths with negligible LO-TO separation, the IR data can be used together with relation (1) to give an estimate of $\epsilon_0/\epsilon_\infty$ also, giving a value of 3.96 ± 0.6 . The discrepancy between these two values is not serious when the possible errors in the frequencies are remembered.

¹⁴ R. H. Lyddane, R. G. Sachs, and E. Teller, *Phys. Rev.* **59**, 673 (1941).

¹⁵ W. Cochran, *Advan. Phys.* **9**, 387 (1960).

¹⁶ W. Cochran and R. A. Cowley, *J. Phys. Chem. Solids* **23**, 447 (1962).

V. CONCLUSION

A factor group analysis of the YAG structure has been performed, showing that there are 98 vibrational modes with $k \approx 0$ belonging to the following irreducible representations:

$$5A_{1u} + 3A_{1g} + 5A_{2u} + 5A_{2g} + 10E_u + 8E_g + 14T_{1g} \\ + 18T_{1u} + 14T_{2g} + 16T_{2u}.$$

15 of the 17 predicted T_{1u} optic modes were observed. The TO and LO frequencies were derived from a K-K analysis of IR reflection data and were shown to satisfy a generalized LST relation. Values for the high- and low-frequency dielectric constants were also obtained. All the A_{1g} and E_g modes together with 11 of the 14 predicted T_{2g} Raman-active modes were observed. Attempts to correlate the motions of the oxygen anions with the modes of free polyhedra showed that a splitting of the modes into internal and external modes was not a good approximation in this crystal.

ACKNOWLEDGMENT

The authors would like to thank L. E. Cheesman for recording the Raman data used in this work.

Acoustic Attenuation in Solids

R. KISHORE

Department of Physics, University of Roorkee, Roorkee, India

(Received 3 April 1968)

With the help of the correlation-function formula given by McLennan, an expression for the viscosity tensor is obtained within the Hartree-Fock approximation using the cubic anharmonic momentum-flux operator. In the Debye approximation for phonons and with a simple expression for relaxation time, solutions are obtained for the coefficients of viscosity at low temperature. These solutions are used to calculate the attenuation of longitudinal and transverse sound waves at 300°K. The calculations are compared with experiment for Ge and Si, and good agreement is found.

INTRODUCTION

IN solids sound waves are damped by thermal conduction and internal friction or viscosity. The correlation-function expression for the viscosity has been obtained by many authors.¹⁻⁴ Here we shall use the expression for the viscosity obtained by McLennan⁴ to calculate the attenuation of sound waves in solids. In the case of insulating solids, a significant contribution to the attenuation of sound waves is due to lattice viscosity which arises from the scattering of phonons. Recently the phonon contribution to the viscosity has

been discussed by several authors,⁵⁻⁹ using the correlation-function formula given by McLennan.⁴ Some authors⁵⁻⁸ have derived the expression for the viscosity by using the harmonic part of the momentum-flux operator, which is the central quantity in the calculation of viscosity. Devault¹⁰ has shown that the harmonic part of the momentum-flux operator vanishes, so all the treatments given by these authors are wrong, and it is necessary to reconsider the problem using the anharmonic momentum-flux operator. Devault⁹ has used the

⁵ G. P. Devault and J. A. McLennan, *Phys. Rev.* **138**, A856 (1965).

⁶ M. J. Rice, *Proc. Phys. Soc. (London)* **89**, 373 (1966).

⁷ P. Gluck, *Proc. Phys. Soc. (London)* **90**, 787 (1967).

⁸ R. Kishore and K. N. Pathak, *Phys. Letters* **25A**, 201 (1967).

⁹ G. P. Devault, *Phys. Rev.* **155**, 875 (1967).

¹⁰ G. P. Devault, *Phys. Rev.* **149**, 624 (1966).

¹ M. S. Green, *J. Chem. Phys.* **22**, 398 (1954).

² R. Kubo, M. Yokota, and S. Nakajima, *J. Phys. Soc. Japan* **12**, 1203 (1957).

³ H. Mori, *Phys. Rev.* **111**, 694 (1958).

⁴ J. A. McLennan, *Advan. Chem. Phys.* **5**, 261 (1968).